The Directional Spectra and Kinematics of Surface Gravity Waves in Tropical Storm Delia

G. Z. FORRISTALL AND E. G. WARD

Shell Development Company, P. O. Box 481, Houston TX 77001

V. J. CARDONE

Oceanweather, Inc., Box 3772, Grand Central Station, New York, NY 10017

L. E. BORGMANN

Statistics Laboratory, University of Wyoming, Laramie 82071

(Manuscript received 31 January 1978, in final form 17 May 1978)

ABSTRACT

Knowledge of the kinematics of the flow beneath surface waves is vital for the design of offshore structures. Due to the technical difficulty of making pertinent measurements in storm conditions, knowledge of the kinematics of storm waves has been based almost entirely on theoretical considerations. Now measurements made with electromagnetic current meters during Tropical Storm Delia have permitted verification of the theories.

There was considerable scatter between the measured velocities and the predictions of unidirectional wave theories, with a clear bias toward overprediction. Use of higher order and irregular unidirectional theories did not substantially improve the comparisons. A good fit with the data could, however, be obtained by using the concept of a directional wave spectrum based on linear wave theory.

The simultaneous wave and particle velocity measurements were used to estimate the directional spectrum through an analysis procedure which took into account the presence of a strong current. The directional spectrum was also hindcast using a numerical model and the comparison of the hindcast with data was good.

The fact that velocity spectra in confused storm seas can be accurately calculated will be directly important in some design problems. In other cases, it is necessary to know the probability distribution of the extreme events. Using the assumption of a Gaussian sea surface, it was possible to satisfactorily predict the distribution of the magnitudes of velocity. All of the comparisons lead to the conclusion that a proper description of storm wave kinematics is dependent on correctly accounting for the directional spreading of the wave energy.

1. Introduction

The calculation of hydrodynamic forces on a fixed structure during a storm requires knowledge not only of wave heights, but also of the subsurface flow due to the waves.

The usual design approach is to use a unidirectional regular wave theory to calculate the velocity and acceleration (kinematics) of the water below the waves and then use a force theory to calculate the forces on structural members due to that water motion. In this paper we will examine the accuracy of wave theories using measured wave kinematics from Tropical Storm Delia.

Due to instrumentation problems and logistic difficulties, measurements of wave kinematics in the ocean have been rather rare. Bowden and White (1966) used the electromagnetic flowmeter developed by the National Institute of Oceanography in the intertidal zone at the mouth of the Mersey River. Later, Simpson (1969) used the same instrument to study waves arriving at the end of a Blackpool pier. Measurements further offshore were made at the Naval Undersea Center oceanographic research tower by Thornton and Krapohl (1974) using Engineering Physics Company flowmeters. Although the 19-m water depth for this experiment was more typical of oceanic conditions than the earlier measurements, the wave field studied was a long low Pacific swell. The measurements during Delia seem to be the first particle velocity measurements made under storm conditions.

The wave theories presently used can be tested by taking the recorded wave height and period and using the theory to predict the horizontal velocity of the water at the depths of the current meters. Comparisons of the predicted and observed velocities show a fair amount of scatter, but also a clear and persistent bias toward overprediction.

To find the source of the overprediction, it is

0022-3670/78/0888-0909$11.00

necessary to discuss the type of wave theory used in design practice. The fundamental difficulty in constructing a mathematical wave theory is the nonlinearity of the free surface boundary conditions. Airy wave theory, which is based on a linearized version of the equations, can be shown to fail to match the known boundary conditions for waves of all but infinitesimal steepness. This failure is so glaring that a great amount of effort has been directed toward producing higher order theories which match the boundary conditions with greater accuracy. The theory most often used in design is Stokes fifth-order theory.

Unfortunately, in the quest for a boundary condition fit, it has been necessary to neglect another known feature of the storm wave field. Nonlinear wave theories all assume that the waves are unidirectional or long-crested. This reduces the problem to two dimensions and makes the mathematical analysis to higher orders possible. In reality, storm waves are extremely confused and short-crested and unidirectional wave theories should not be expected to apply.

It is useful to think of an irregular sea as being made up of the sum of many small, regular component wavelets, each having a different amplitude, frequency and direction of travel, and a random phase angle. Now consider two wavelets with the same amplitude, but different frequencies and phase angles, traveling in exactly opposite directions. At certain points on the sea surface, the crests of both wavelets will coincide, producing a wave height with the sum of their amplitudes. However, below those points, the water velocities will be in opposite directions and tend to cancel. This is the basis for the scatter in the comparisons of observed and predicted velocities.

Now if one of the wavelets travels east and the other north, the vector addition of the velocities from the two will never produce a velocity magnitude as large as if they were traveling in the same direction. Since the component wavelets will have many directions and frequencies in a real storm sea, these effects will conspire to produce a bias toward overprediction in any unidirectional wave theory.

Progress is being made in understanding nonlinear effects in directionally spread seas (e.g., Weber and Barrick, 1977), but no practical method for calculating wave kinematics yet exists for such a theory. However, because of the linearity of Airy theory, it can be extended through spectral concepts to realistically model many attributes of the irregular sea. The pertinent question is thus whether the assumption of unidirectionality or linearity is the most damaging. We will show that during Tropical Storm Delia much better agreement can be reached by using a linear theory which accounted for the directional nature of the measured waves.

First, we briefly describe the measurements made during Delia. Then, individual high waves in the record are analyzed using Stokes fifth-order theory which generally overpredicts the measured velocities. Tests of irregular unidirectional theories produced no substantial improvement in comparisons.

Using the simultaneous wave staff and current meter records, it was possible to estimate the directional spectrum of the waves, although the presence of a strong current introduced some complications into the analysis. One of the products of the analysis is an assessment of the accuracy of the linear transfer function between wave height and particle velocity. Since the accuracy is rather good, the transfer function may be used to calculate velocity spectra given the wave directional spectrum.

Directional spectra can be hindcast using numerical models such as the one described by Cardone *et al.* (1976), but there has been little verification of the directional characteristics of the hindcast spectra for storms. Thus, we made a hindcast of Delia and found that the agreement between the hindcast and measured directional spectra was quite good.

The fact that the velocity spectrum in confused seas can be calculated from linear theory will be directly useful in studying the fatigue life of offshore structures. However, for design work, it is also necessary to know the magnitudes of the extreme events which the structure must endure and the spectrum does not provide that information directly. We thus calculate the probability distribution of the velocity magnitudes based on the wave height spectrum and compare them with the observed velocity distributions. This approach is also successful.

During Tropical Storm Delia, a linear wave theory which accounts for the directional spreading of the waves was able to accurately predict both the velocity spectrum and the extreme speed distribution. On the other hand, a nonlinear regular wave theory consistently overpredicted the velocities under individual high waves. The implication is that a proper description of storm wave kinematics is more dependent on correctly accounting for the directional spreading of the waves than on correctly matching the nonlinear boundary condition.

2. Measurements during Delia

The measurements of wave kinematics were made at the Buccaneer oil and gas production platform located at 28°53′28″ N, 94°41′42″ W. The instrumentation system and preprocessing of the data were described in some detail by Forristall *et al.* (1977), but it is useful to repeat the most important points here. The wave staff and a string of three electromagnetic current meters are mounted at the center of a 200 ft bridge between two pile-supported struc-

FIG. 1. Current meters being lowered into the water next to the wave staff at the Buccaneer A platform.

tures. Fig. 1 shows two of the current meters being lowered into the water on a pair of taut wires located 6 ft north of the wave staff. During Delia, the current meter sensors were located 55, 35 and 10 ft from the bottom and the water depth was 68 ft.

The instrumentation performed well during the storm. However, we discovered a few months later that the anchor holding the bottom of the taut wire pair had rotated 31° in a scour pit. It has been impossible to determine when the rotation occurred, although it was most likely during the storm. Discrepancies between the direction of wave travel calculated separately from the three current meters suggest motion of the taut wire system after 1500 CDT 4 September. However, no consistent pattern could be found and it is possible that the system was rotating in a pendulum mode during the latter stages of the storm. The analysis of the current meter records was thus done without any rotation correction and it must be recognized that there is some uncertainty in the reported velocity directions.

The data were recorded in the field on two 7-track analog FM tape recorders running at 0.03 inch per second (ips). The field tapes were later digitized at a playback speed of 7.5 ips with a sampling rate of 500 Hz and a 160 Hz antialiasing filter. The corresponding real-time rates were 2 Hz digitization and 0.64 Hz filtering. The digitized records were converted to engineering units using the automatic calibration signals written on the field tape and a cosine response correction equation was applied to the current meter signals.

The records from the current meters contained motions of two widely separated time scales: oscillatory motion associated with the waves and much more slowly varying currents. To separate out the oscillatory motion for study of the waves, we applied the 249-point numerical filter described by Forristall *et al.* (1977) as a high-pass rather than a low-pass filter. It might be thought that associating only oscillatory motions with waves would remove one possible source of nonlinearity: the Stokes drift. However, the transport of water due to the Stokes drift can be seen only in Lagrangian measurements. Measurements of Stokes waves in a fixed Eulerian frame will include only oscillatory motions.

The fact that the wave and particle velocity data were recorded on two different tape recorders caused some difficulty in the analysis. The two tape recorders ran at slightly different speeds (<0.5% difference). This introduced a discrepancy between the two data series which was on the order of 15 seconds per hour. It was therefore necessary to correct the data to provide time correlation between wave height and particle velocity. Fortunately, the hour and minute marks written on each of the two tapes by the same clock made such corrections possible. Using the minute marks, each record was interpolated so that there were precisely 120 digitized values between minute marks and the minute marks on each tape were then synchronized. The records are thus accurately aligned within the 0.5 s digitization interval. The particle velocity data also had to be corrected for the low-pass filter of the current meter electronics. This correction, which was very small at the frequencies of interest, was accomplished numerically by applying the inverse of the analytical description of the filter to the particle velocity data.

3. Unidirectional wave analysis

In developing unidirectional wave theories, it is assumed that all wave energy travels or propagates in a single direction. From this assumption, it follows that the horizontal components of wave-induced velocities and accelerations are unidirectional and colinear with the direction of energy propagation. These theoretically described waves are sometimes referred to as infinitely long-crested since the unidirectionality implies that there are no variations in wave properties perpendicular to the direction of wave travel. Unidirectional wave theories can be classified as being either regular or irregular.

a. Regular wave theories

Regular wave theories describe waves which are periodic in space and time. The resulting wave profiles are symmetric about the wave crest position and propagate without deformation or change. The solution to a regular wave theory is completely specified by the wave height (or alternatively, crest elevation), wave period and water depth. For these specified parameters, a given regular wave theory produces a unique surface profile and subsurface kinematics. It is particularly important to note that characteristics of the wave profile solution, such as wave shape and the ratio of crest elevation to wave height, are uniquely determined by the choice of wave theory and the specified height, period and depth.

The simplest example of a regular unidirectional wave theory is the familiar Airy or linear wave theory. This theory is based on a linearization of the free surface boundary condition (pressure at the wave profile surface). The resulting solution to the wave equation produces a wave theory which is characterized by a single harmonic function. The resulting wave profile is sinusoidal. Due to the linearization involved, this theory is strictly applicable only to small amplitude waves of infinitesimal steepness.

To remove this restriction, various higher order nonlinear regular wave theories have been developed. These theories are based on methods for approximating the nonlinear free surface boundary conditions. Examples of such theories include the Stokes fifth-order and Chappelear (1961) theories, the regular streamfunction theory (Dean, 1965), and the diagonal matrix version of the extended velocity potential or EXVP-D theory (Lambrakos and Brannon, 1974).

Nonlinear regular unidirectional wave theories are currently used in most analyses of static platform loads under storm wave conditions. Results presented by Lambrakos and Brannon (their Fig. 8) indicate that the Stokes fifth-order, regular streamfunction and EXVP-D wave theories predict essentially the same velocities for the same specified profile. Therefore, within appropriate limits on wave height and period, these theories predict similar results. From the standpoint of engineering application, there is apparently little basis to prefer one theory over another.

b. Irregular wave theories

Observed wave profiles frequently have irregular profiles which are not periodic in time. This observed lack of regularity has led to concern over the validity of applying regular wave theories to irregular waves and has motivated the development of several irregular wave theories. Irregular wave theories provide solutions for wave-induced velocities and acceleration which are based on a completely prescribed surface profile, as opposed to the simpler wave height and period specification required for regular wave theories. Both nonlinear and linear irregular wave theories have been developed.

Examples of nonlinear irregular wave theories include the irregular streamfunction (Dean, 1965) and extended velocity potential or EXVP (Lambrakos and Brannon, 1974) theories. These nonlinear irregular wave theories again provide solutions to the wave equation which approximately satisfy the nonlinear free surface boundary condition, but force the predicted wave profile to match the prescribed profile. The wave profile is assumed to propagate without deformation in the irregular streamfunction wave theory. The EXVP wave theory provides for deformation of the profile as it propagates.

A linear irregular unidirectional wave theory can be developed based upon the linear superposition of a number of linear or Airy waves. Basically, this approach begins with a Fourier analysis of the desired wave profile which provides the amplitudes and phases of the harmonic components. Linear wave theory is assumed to be applicable to each harmonic component and the principle of superposition is used to add the wave solutions for the components. The resulting solution provides the wave-induced velocities and accelerations for the desired wave profile. Note that such a linear irregular unidirectional wave theory is an obvious simplification of the directional wave theory described in later sections of this report. Linear irregular unidirectional wave theories based on the above principles have been published (Wheeler, 1970; Jahns and Wheeler, 1973). Both of these theories use an empirically motivated scaling of the vertical coordinate in the depth decay function. Additionally, Wheeler's theory forces all harmonic components to propagate at the same velocity so that the waves propagate without deformation.

c. Comparison of predicted and measured velocities

We now proceed to compare measured wave induced velocities with those predicted by unidirectional wave theories. The main emphasis is on Stokes fifth order theory. Some comparisons with irregular unidirectional wave theories are also included.

A sample of the processed data which includes the highest wave measured in Delia is shown in Fig. 2. The top trace in the figure is the wave profile, with the maximum distance between a crest and the preceding trough equal to 24.4 feet. The period of that wave, defined as the time between zero downcrossings, was 8.0 s. The next six traces are the eastward and northward components of the particle

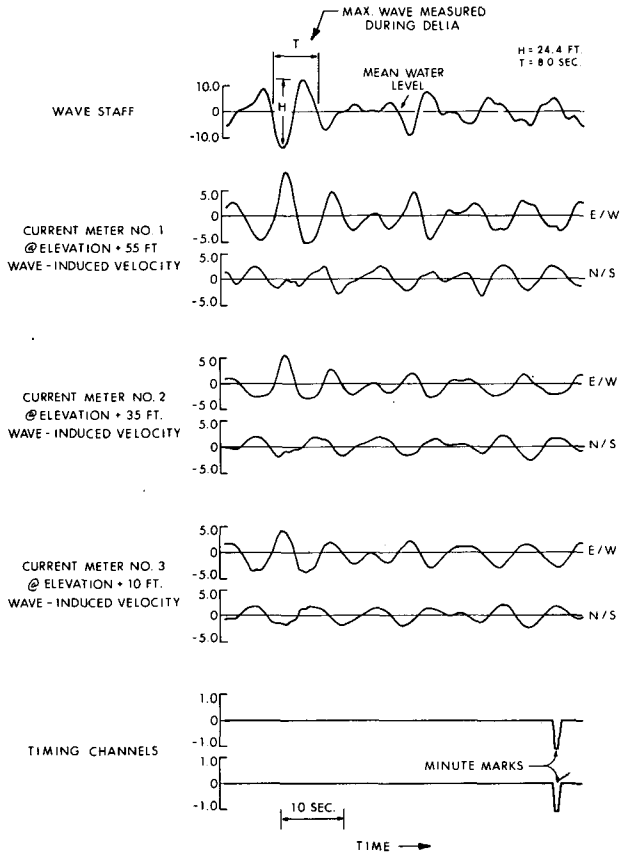

FIG. 2. Sample wave staff and current meter data including the largest wave measured in Delia.

velocity records, with the eastward component of the top current meter nearest the top of the figure.

Although most of the water velocity associated with the largest wave was in the east-west direction, the north-south component was not negligible. The complicated nature of the flow field can be seen more clearly in Fig. 3, where the vector velocity at the top current meter has been plotted. The line traces the history of the top of the velocity vector, with the numbers giving the time in seconds since the start of the record in Fig. 2. Since the velocity is definitely not unidirectional, some judgment is called for in a comparison of the data to a unidirectional wave theory. To give the unidirectional wave theory the fairest test, we based the comparison on the magnitude of the vector velocity.

The properties of a Stokes fifth-order wave with a height of 24.4 ft and a period of 8.0 s were determined and compared with the observations as shown in Fig. 4. The calculated wave profile is somewhat different from that measured, having a sharper crest. The velocities at the three current meter depths show a consistent tendency toward overprediction under the crests. Note, too, that the peaks of the observed velocity magnitude traces are much broader than the calculated peaks. This feature is associated with the elliptical nature of observed velocity vectors as shown in Fig. 3.

Because some scatter in the comparison of observed and predicted wave properties is to be expected, it is important to examine a number of individual waves to see if any consistent trends can be found. Since we are most interested in extreme values, we selected the largest wave in each 30 min segment of the data from 0600 to 1400 CDT for analysis. The solid line in Fig. 5 shows the maximum wave height determined for each 30 min segment. For each wave, we compared and observed and predicted peak velocity magnitudes under the crest and trough of the wave. Precise time synchrony was not required. The observed velocity magnitude maximum nearest the crest or trough was used, although the time of the maximum was almost always within 1.0 s of the crest or trough.

The predicted versus measured velocities for the 16 waves are shown in Figs. 6, 7 and 8 for the top, middle and bottom current meters, respectively. Most of the velocities under the crests are overpredicted, particularly for the upper two meters. The velocities under the wave troughs are also generally overpredicted for the lower two meters. The velocities under the troughs at the uppermost meter indicate a scatter of over- and underpredictions. Plots of the ratios of predicted to measured velocity versus wave steepness revealed no noticeable trends.

It is not clear from Fig. 4 how much of the error in velocity prediction is due to the mismatch between the measured irregular profile and the regular profile calculated using the Stokes theory. Therefore, we also analyzed this wave using the irregular streamfunction theory. These results are also compared with the measurements and Stokes results in Fig. 4. Under the wave crest, the irregular streamfunction theory overpredicts the measured velocity as did the regular Stokes theory. The amount of overprediction by the irregular theory is slightly less than that due to the regular theory, but the overall trends of the two solutions are quite similar. These results suggest that errors in predicted velocities are not strongly influenced by either the agreement (irregular streamfunction) or lack of agreement (Stokes) between the predicted and measured wave profiles. This suggestion is also supported by analysis of several of the large waves whose profiles were closely approximated by Stokes theory. The overprediction trends for these waves were similar to the results shown in Fig. 4.

A sample comparison of linear irregular unidirectional theory with the data is also shown in Fig. 4. The agreement between the linear irregular theory and the nonlinear regular and irregular theories is somewhat surprising. The amount of overprediction

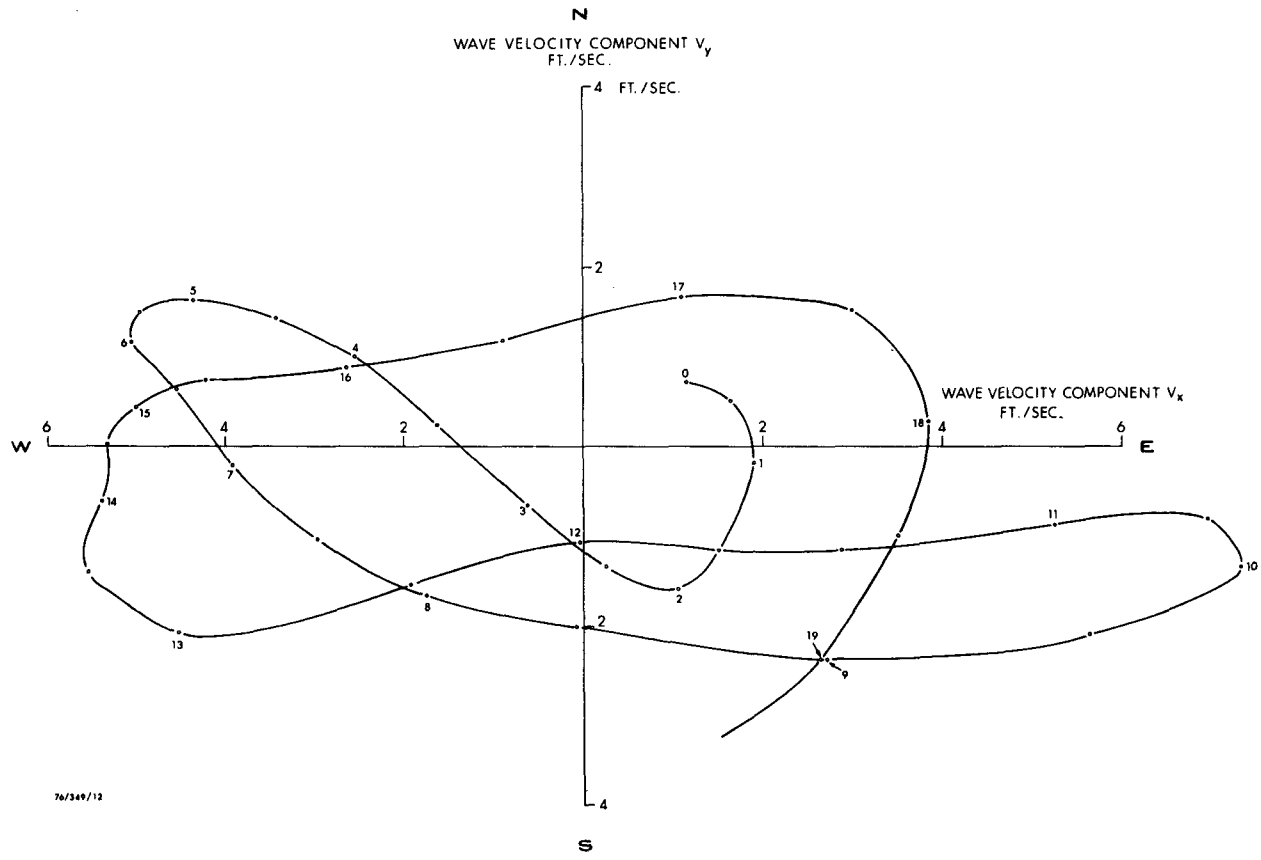

FIG. 3. Time history of the horizontal velocity measured at the top current meter during the largest wave. Numbers on curve give the time in seconds after the start of Fig. 2.

in velocity under the wave crest is similar to that from using the regular and irregular nonlinear theories. These results again suggest that errors in predicted velocities are not due to a mismatch between measured and predicted wave profiles.

A final consideration of regular versus irregular wave theories is based on work reported by Lambrakos and Brannon. They performed a theoretical comparison of the regular Stokes fifth-order and irregular EXVP wave theories. The comparison examined the importance of specifying both wave height and crest elevation which is possible with irregular theories. Using the EXVP theory, velocities were predicted for waves of fixed height and period, but different crest elevations. These EXVP predictions were compared to the Stokes solution for the same height and period which, of course, had a single unique crest elevation. The comparison indicated that the Stokes theory would overpredict velocities under wave crests whenever it overpredicted the crest elevation. This trend agrees with the wave shown in Fig. 4. However, when all the 30 min maximum waves were considered, no clear trend toward this sort of behavior was discernible.

d. Summary of comparisons

Measured wave-induced velocities have been compared with velocities predicted by a unidirectional regular nonlinear wave theory. Significant errors are observed in the predicted velocities. The theory overpredicts velocities. The amount of overprediction is most severe under the wave crests, particularly at elevations nearer the free surface. The theory used in the comparisons was Stokes fifth-order theory. Evidence indicates that several popular theories produce similar results.

The irregularity of observed ocean wave profiles was examined as the cause of the observed overpredictions. Both nonlinear and linear unidirectional irregular wave theories were considered. Irregular theories can describe observed wave profile irregularities in contrast to regular theories which can describe only the height and period of the observed wave. However, the errors in velocities predicted by irregular theories are similar to those produced by regular theories. Thus, the irregularity of observed waves does not appear to be the cause of the errors in predicted velocities.

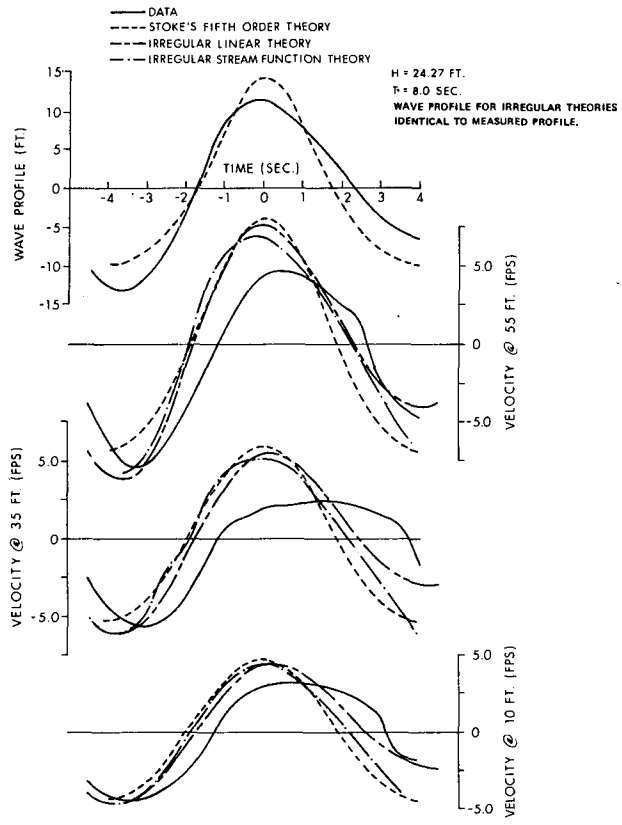

FIG. 4. Comparison of Stokes and irregular unidirectional wave theories to measurements made during the largest wave. Note that the irregular theories match the surface profile exactly.

4. Directional wave analysis

a. Wave and velocity spectra

An intuitive idea of the reason for the over-predictions of unidirectional wave theory may be gained from a study of Fig. 3. Some of the energy of the wave is causing motion transverse to the main wave direction which does not contribute fully to the peak velocity magnitude. We might hope that the task of calculating the kinetic energy levels at the various depths would be somewhat easier than calculating the peak velocities and still provide a test of the appropriateness of a wave theory. Such calculations can be performed using linear wave theory and power spectral techniques.

As shown by Bowden and White (1966), data from a wave staff and an electromagnetic current meter are sufficient to estimate the directional wave spectrum. Nagata (1964) has also developed the applicable theory. During the analysis, a natural

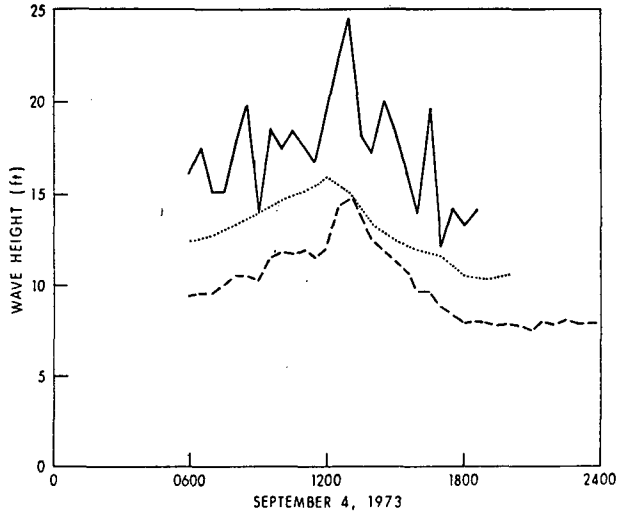

FIG. 5. Delia wave height history. Solid line: 30 min maximum wave heights; dashed line: measured significant wave height; dotted line: hindcast significant wave height.

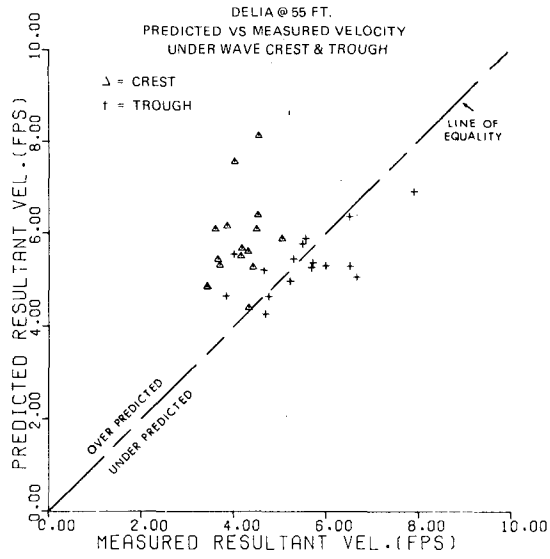

FIG. 6. Comparison of Stokes fifth-order to measured maximum velocities during the largest waves for top current meter.

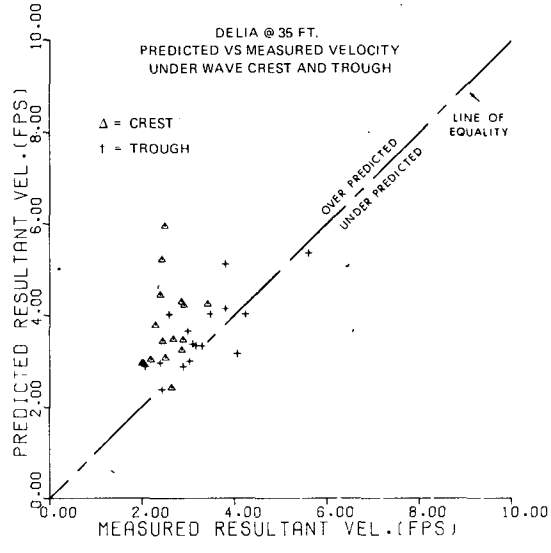

FIG. 7. As in Fig. 6 except for the middle current meter.

check on the accuracy of the linear transfer function between height and velocity appears. In addition, the measured directional spectra provide a rare opportunity to check a numerical scheme for hindcasting directional spectra. One complication not considered by Bowden and White arose in the analysis—the presence of a strong current. During Tropical Storm Delia, the maximum measured near surface current was 7 ft s^{-1} (Forristall, *et al.*, 1977). The strength of this current compels consideration of possible wave-current interaction.

b. Wave-current interaction

It is well known that when a train of waves propagates through a region of slowly varying currents, waves are conserved (Phillips, 1977, p. 57). For the simple case of a train of regular waves propagating in the direction of a slowly varying current, this conservation of waves is expressed by

$$n = f + uk/2\pi = \text{constant}, \quad (1)$$

where n is the reciprocal of the number of waves passing a fixed point per unit time, f is the wave frequency measured in a coordinate system moving with the current, u is the current velocity, and k is the wave number given by the dispersion relationship

$$(2\pi f)^2 = gk \tanh(kd), \quad (2)$$

where g is the gravitational acceleration and d is the water depth.

The wave current interaction described by (1) is purely kinematic and does not describe any changes in wave energy. Such energy exchanges between waves and currents are predicted from consideration of the dynamics of either linear wave theory (Phillips, 1977) or higher order wave theories which include nonlinear effects (Longuet-Higgins and Stewart, 1960), but will not be dealt with here.

By definition, n is the wave frequency (f_0) perceived by a fixed observer, so

$$f_0 = f + uk/2\pi. \quad (3)$$

Eq. (3) provides the relationship between wave frequencies perceived by a fixed observer and an observer moving with the current. This Doppler shift is purely an effect of the measurement frame and does not describe any physical modification of the waves by the current. Wave theories are formulated in a coordinate frame in which the current is zero; i.e., the only velocities predicted by wave theories are those associated with the wave-induced motion. In the case where waves exist in the presence of a current, the coordinate frame of the wave theory moves with the current. For the linear wave theory upon which the calculation of the directional spectrum is based, the dispersion relationship given by Eq. (2) relates the wavenumber to the frequency f in the moving coordinate system. However, the

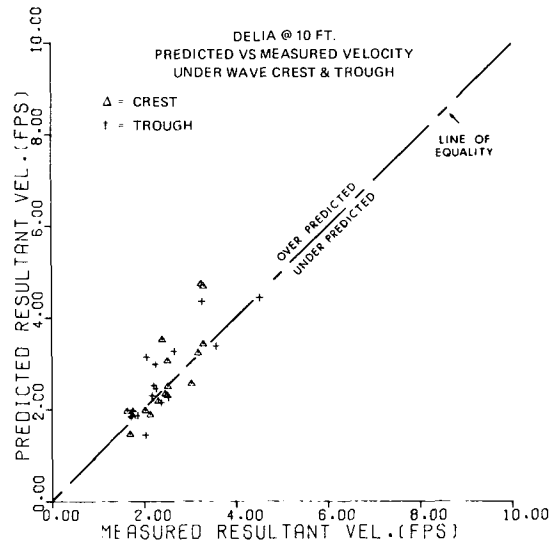

FIG. 8. As in Fig. 6 except for the bottom current meter.

fixed wave staff and current meter array measures waves of apparent frequency f_0. Thus, to properly estimate directional spectra using the linear dispersion relationship, we must account for the frequency shift given by Eq. (3). The result of the calculations will be the directional spectrum in the coordinate frame moving with the current. This is the spectrum that could be related to a wavenumber spectrum estimated from aircraft or spacecraft observations.

c. Hindcast directional spectra

The directional spectrum in the moving frame is needed in applications since the wave theory holds true in that frame and thus can be used to calculate wave velocities and accelerations from the spectrum. It is not apparent that the wave hindcast model described by Cardone *et al.* (1976) and used in this study should do a reasonable job of hindcasting that directional spectrum, since it explicitly includes neither the kinematic nor the dynamic wave-current interactions. However, some heuristic arguments can be made which indicate the possibility of success, which has been partially demonstrated in previous comparisons of hindcast and measured wave data (Cardone *et al.*, 1976).

The wave-current interactions should have the most effect toward the high-frequency end of the spectrum. However, the high-frequency tail of the spectrum is dependent mainly on the local wind and is limited by a fully developed spectral form which has empirically included wave-current interactions. Those spectral components which are governed only by nearby conditions will have no chance to be modified by spatially variable currents and should be correctly specified by the hindcast model. Spectral components which propagate from far away where the current was substantially different will

be modified by the variable current. However, these components will typically be the lower frequency components on which the wave-current interactions have the least effect.

The previous verifications of the hindcast model were based on wavestaff measurements which allowed only comparison of the wave spectra, that is, total wave energy and the energy distribution as a function of wave frequency (Cardone *et al.*, 1976). Since current data were not available, the effect of wave-current interaction could not be included. The hindcast and measured total energy as measured by the total variance or significant wave height compared satisfactorily, particularly at peak storm conditions. Since the Doppler shift expressed by Eq. (3) does not affect total wave energy, this aspect of the previous verification will remain unchanged. The comparisons of hindcast and measured energy frequency distributions were generally favorable, again particularly near peak storm conditions, but a tendency for hindcast energy to exceed measured energy at the lower frequency bands has been observed. As will be shown later, accounting for the Doppler shift in the measured wave spectra tends to increase the energy at lower frequencies, but the magnitude of this increase is not sufficient to completely explain this tendency of the hindcasts.

During a hurricane, the currents and the waves are both being generated by strong winds at the same time. Although it would be preferable to couple the wave hindcast model with a wind-driven current model and include wave-current interactions explicitly, the above arguments show that there is some hope of success even neglecting the interactions. The comparisons between hindcasts and measurements show that this hope is justified.

5. Estimation of directional spectra in the presence of currents

The goal of this development is the calculation of the directional spectral density in a coordinate frame which moves with the current from measurements of water surface elevation and water particle velocity in a fixed coordinate frame. Cartwright (1963) studied the similar problem of calculating the spectrum of encounter of a ship moving through directionally spread waves. The present problem can be thought of as the inverse of the one he studied and is somewhat more difficult. We proceed by first expressing the familiar equations for wave theory in the moving frame. Next, the transformation from the moving frame to a fixed frame is introduced and used to express the wave theory relative to the fixed frame in which the measurements were made. The transformed wave theory is then used to develop a procedure for calculating the directional spectral densities relative to a fixed frame from the cospectra of the measurements. Finally, the directional spectral density in the moving frame is obtained from the density relative to the fixed frame by applying the inverse of the transformation.

a. Moving coordinate frame wave theory

We assume that the water surface elevation in a coordinate frame moving with the current may be described as

$$\eta(x,y,t) = \sum_m \sum_n A_{mn} \cos\psi_{mn}(x,y,t), \tag{4}$$

where

$$\psi_{mn}(x,y,t) = k_m x \cos\theta_n + k_m y \sin\theta_n - 2\pi f_m t + \phi_{mn} \tag{5}$$

$$A_{mn} = 2[S(f_m,\theta_n)\Delta f_m \Delta\phi_n]^{1/2}, \tag{6}$$

and

- (x,y,z) rectangular coordinate system which moves with the current. The origin is at the sea floor and x is positive northward, y positive eastward and z positive upward
- f_m wave frequency in cycles per second (Hz)
- k_m wavenumber associated with frequency f_m
- θ_n direction the wavelet is traveling as measured clockwise from the x axis
- ϕ_{mn} a random phase for the (m,n) wavelet, assumed to be uniformly distributed over the angles $(0,2\pi)$ and independent from wavelet to wavelet
- A_{mn} amplitude of the (m,n) wavelet
- $S(f,\theta)$ directional spectral density at frequency f and direction of travel θ
- Δf_m frequency interval about frequency f_m
- $\Delta\theta_n$ angle interval about travel direction θ_n.

We further assume that the kinematics of the waves described by (4) can be obtained from linear wave theory so that

$$V_x(x,y,z,t) = \sum_m \sum_n A_{mn} 2\pi f_m \frac{\cosh k_m z}{\sinh k_m d} \times \cos\theta_n \cos\psi_{mn}(x,y,t), \tag{7}$$

$$V_y(x,y,z,t) = \sum_m \sum_n A_{mn} 2\pi f_m \frac{\cosh k_m z}{\sinh k_m d} \times \sin\theta_n \cos\psi_{mn}(x,y,t), \tag{8}$$

where $V_x(x,y,z,t)$ is the x component of the water particle velocity at space location (x,y,z) and at time t, and $V_y(x,y,z,t)$ the y component of the water particle velocity.

b. Fixed coordinate frame

Let the current have a vector velocity (as measured in the fixed frame) equal to (T_x,T_y). The current is assumed to be uniform with depth so that

it acts as a simple translation of the frame in which the wave theory applies. In Delia, the current was nearly uniform with depth, so the value of the current at the top current meter was used in the analysis. It might be possible to treat more complicated situations by depth-averaging the current in the manner suggested by Stewart and Joy (1974).

The fixed frame measurements are thus being made in a coordinate system moving at velocity $(-T_x, -T_y)$ with respect to the frame of Eq. (4). If the measurement site is located at (x_0,y_0) in the moving frame at time $t = 0$, then the measurement site location as a function of time is given by

$$x' = x_0 - T_x t, \tag{9}$$

$$y' = y_0 - T_y t. \tag{10}$$

1) Wave theory

Substituting Eqs. (9) and (10) into (4) and (5), the water surface elevation with respect to the fixed frame becomes

$$\eta(x',y',t) = \sum_m \sum_n A_{mn} \cos\psi_{mn}(x',y',t), \tag{11}$$

where

$$\psi_{mn}(x',y',t) = k_m x_0 \cos\theta_n + k_m y_0 \sin\theta_n + \phi_{mn} - (2\pi f_m + k_m T_x \cos\theta_n + k_m T_y \sin\theta_n)t. \tag{12}$$

The water particle velocities will have a similar substitution of $\psi_{mn}(x',y',t)$ for $\psi_{mn}(x,y,t)$.

2) Cross-covariances

The cross-covariances of these quantities measured in the fixed frame can be formed by taking lagged products and passing from summation to integration:

$$C_{\eta\eta}(\tau) = 2\int_0^\infty \int_0^{2\pi} S(f,\theta) \cos 2\pi[\tau\beta(f,\theta)]d\theta df, \tag{13}$$

$$C_{\eta V_x}(\tau) = 2\int_0^\infty \int_0^{2\pi} S(f,\theta)Q(f) \cos\theta \times \cos 2\pi[\tau\beta(f,\theta)]d\theta df, \tag{14}$$

$$C_{\eta V_y}(\tau) = 2\int_0^\infty \int_0^{2\pi} S(f,\theta)Q(f) \sin\theta \times \cos 2\pi[\tau\beta(f,\theta)]d\theta df, \tag{15}$$

$$C_{V_xV_x}(\tau) = 2\int_0^\infty \int_0^{2\pi} S(f,\theta)Q^2(f) \cos^2\theta \times \cos 2\pi[\tau\beta(f,\theta)]d\theta df, \tag{16}$$

$$C_{V_xV_y}(\tau) = 2\int_0^\infty \int_0^{2\pi} S(f,\theta)Q^2(f) \cos\theta \sin\theta \times \cos 2\pi[\tau\beta(f,\theta)]d\theta df, \tag{17}$$

$$C_{V_yV_y}(\tau) = 2\int_0^\infty \int_0^{2\pi} S(f,\theta)Q^2(f) \sin^2\theta \times \cos 2\pi[\tau\beta(f,\theta)]d\theta df, \tag{18}$$

where

$$Q(f) = 2\pi f \frac{\cosh kz}{\sinh kd}, \tag{19}$$

$$\beta(f,\theta) = f + (1/2\pi)k(T_x \cos\theta + T_y \sin\theta). \tag{20}$$

3) Coordinate transformation

To recognize Eqs. (13)–(18) as Fourier transforms of power spectra, we introduce a change of variables in the integration given by

$$\tilde{f} = \beta(f,\theta), \tag{21}$$

$$\tilde{\theta} = \theta. \tag{22}$$

This change of variables is a logical consequence of the coordinate transformation given by Eqs. (9) and (10) as expressed in Eq. (12). Note that $\tilde{f}$ or $\beta(f,\theta)$ is the frequency in the fixed coordinate frame, which is a function of the angle θ. The frequency $\tilde{f}$ corresponds to f_0 introduced in Eq. (2) [cf. Eqs. (2) and (20)]. However, (20) is a more general expression than (2) since it indicates the angular dependence which arises when the direction of wave propagation is not colinear with the current velocity.

The Jacobian of the transformation expressed in (21) and (22) is given by

$$\frac{\partial\beta}{\partial f} = 1 + \frac{4\pi f(T_x \cos\theta + T_y \sin\theta)}{g(\tanh kd + kd\,\mathrm{sech}^2 kd)}. \tag{23}$$

For currents opposed to the direction of wave propagation, there exists a frequency high enough that the Jacobian is zero. To see the consequences of this more clearly, let $-u = T_x \cos\theta + T_y \sin\theta$ and make the deep water approximation for wavenumber such that

$$\frac{\partial\beta}{\partial f} = 1 - (4\pi f u/g). \tag{24}$$

The frequency for which the Jacobian is zero is then

$$f^* = g/4\pi u \tag{25}$$

and for this frequency the phase speed of a wave is given by

$$C^* = g/2\pi f^* = 2u. \tag{26}$$

Substituting Eq. (25) in the deepwater version of (21) yields

$$\tilde{f} = f\left(1 + \frac{f}{2f^*}\right). \tag{27}$$

From Eq. (27), we note that frequencies f in the interval $[f^*,2f^*]$ would be mapped into the same range as frequencies in the interval $[0,f^*]$. Increasing frequencies f in the interval $[f^*,2f^*]$ would result in decreasing frequencies $\tilde{f}$. Waves with frequencies

$f > 2f^*$ would have phase speeds less than u indicating an apparent propagation against the wavenumber vector ($\tilde{f} < 0$).

Thus, the transformation given by (21) can be properly executed only over one frequency branch. This restriction is not very serious in practice since even for strong currents, f^* will be rather high ($u = 5$ ft s^{-1} corresponds to $f^* = 0.51$ Hz). Furthermore, on physical grounds, it is unlikely that any significant amount of high-frequency wave energy will travel in a direction opposing the current. Thus, we make the assumption that $S(f,\theta)$ is zero for $f > f^*$ and proceed with the analysis.

For subsequent use, we note that for $f \in [0,f^*]$ there exists an inverse function such that

$$f = \beta^{-1}(\tilde{f},\tilde{\theta}). \tag{28}$$

Eq. (28) can be evaluated by combining (2) and (20) with (21) and solving by successive approximations.

4) Cospectral densities

We now define

$$\tilde{S}(\tilde{f},\tilde{\theta}) = S[\beta^{-1}(\tilde{f},\tilde{\theta}),\tilde{\theta}](\partial\beta/\partial f)^{-1} \tag{29}$$

and

$$\tilde{Q}(\tilde{f},\tilde{\theta}) = Q[\beta^{-1}(\tilde{f},\tilde{\theta})]. \tag{30}$$

With these definitions and the change of variables discussed in the previous section, Eqs. (13)–(18) for the cross covariances can be expressed as

$$C_{\eta\eta}(\tau) = 2\int_0^\infty \cos 2\pi\tilde{f}\tau d\tilde{f} \int_0^{2\pi} \tilde{S}(\tilde{f},\tilde{\theta})d\tilde{\theta}, \tag{31}$$

$$C_{\eta V_x}(\tau) = 2\int_0^\infty \cos 2\pi\tilde{f}\tau d\tilde{f} \int_0^{2\pi} \tilde{S}(\tilde{f},\tilde{\theta})\tilde{Q}(\tilde{f},\tilde{\theta}) \cos\tilde{\theta}\delta\tilde{\theta}, \tag{32}$$

$$C_{\eta V_y}(\tau) = 2\int_0^\infty \cos 2\pi\tilde{f}\tau d\tilde{f} \int_0^{2\pi} \tilde{S}(\tilde{f},\tilde{\theta})\tilde{Q}(\tilde{f},\tilde{\theta}) \sin\tilde{\theta}d\tilde{\theta}, \tag{33}$$

$$C_{V_xV_x}(\tau) = 2\int_0^\infty \cos 2\pi\tilde{f}\tau d\tilde{f} \int_0^{2\pi} \tilde{S}(\tilde{f},\tilde{\theta})\tilde{Q}^2(\tilde{f},\tilde{\theta}) \cos^2\tilde{\theta}d\tilde{\theta}, \tag{34}$$

$$C_{V_xV_y}(\tau) = 2\int_0^\infty \cos 2\pi\tilde{f}\tau d\tilde{f} \int_0^{2\pi} \times \tilde{S}(\tilde{f},\tilde{\theta})\tilde{Q}^2(\tilde{f},\tilde{\theta}) \cos\tilde{\theta} \sin\tilde{\theta}d\tilde{\theta}, \tag{35}$$

$$C_{V_yV_y}(\tau) = 2\int_0^\infty \cos 2\pi\tilde{f}\tau d\tilde{f} \int_0^{2\pi} \tilde{S}(\tilde{f},\tilde{\theta})\tilde{Q}^2(\tilde{f},\tilde{\theta}) \sin^2\tilde{\theta}d\tilde{\theta}. \tag{36}$$

These expressions for the cross covariances are now recognizable as the Fourier transforms of the cospectral (c_{xy}) and quadspectral (q_{xy}) densities since

$$C_{xy}(\tau) = 2\int_0^\infty c_{xy} \cos 2\pi f\tau df + 2\int_0^\infty q_{xy} \sin 2\pi f\tau df. \tag{37}$$

Therefore, we can write by inspection

$$c_{\eta\eta}(\tilde{f}) \equiv \tilde{S}(\tilde{f}) = \int_0^{2\pi} \tilde{S}(\tilde{f},\tilde{\theta})d\tilde{\theta}, \tag{38}$$

$$c_{\eta V_x}(\tilde{f}) = \int_0^{2\pi} \tilde{S}(\tilde{f},\tilde{\theta})\tilde{Q}(\tilde{f},\tilde{\theta}) \cos\tilde{\theta}d\tilde{\theta}, \tag{39}$$

$$c_{\eta V_y}(\tilde{f}) = \int_0^{2\pi} \tilde{S}(\tilde{f},\tilde{\theta})\tilde{Q}(\tilde{f},\tilde{\theta}) \sin\tilde{\theta}d\tilde{\theta}, \tag{40}$$

$$c_{V_xV_x}(\tilde{f}) = \int_0^{2\pi} \tilde{S}(\tilde{f},\tilde{\theta})\tilde{Q}^2(\tilde{f},\tilde{\theta}) \cos^2\tilde{\theta}d\tilde{\theta}, \tag{41}$$

$$c_{V_xV_y}(\tilde{f}) = \int_0^{2\pi} \tilde{S}(\tilde{f},\tilde{\theta})\tilde{Q}^2(\tilde{f},\tilde{\theta}) \cos\tilde{\theta} \sin\tilde{\theta}d\tilde{\theta}, \tag{42}$$

$$c_{V_yV_y}(\tilde{f}) = \int_0^{2\pi} \tilde{S}(\tilde{f},\tilde{\theta})\tilde{Q}^2(\tilde{f},\tilde{\theta}) \sin^2\tilde{\theta}d\tilde{\theta}. \tag{43}$$

5) Directional spectra estimation

The left-hand sides of Eqs. (38)–(43) can be found directly from the fixed frame measurements. At each frequency, we thus have six integral measures of the transformed directional spectrum from which we desire to learn something about the spectrum. Given the form of the integrals, it is natural to express the directional dependence as a truncated Fourier series of the spreading function $\tilde{H}(\tilde{f},\tilde{\theta})$. Therefore, let

$$\begin{aligned}\tilde{S}(\tilde{f},\tilde{\theta}) &= \tilde{S}(\tilde{f})\tilde{H}(\tilde{f},\tilde{\theta}) \\ &= \tilde{S}(\tilde{f})[a_0(\tilde{f})/2 + a_1(\tilde{f}) \cos\tilde{\theta} + a_2(\tilde{f}) \cos 2\tilde{\theta} \\ &\qquad + b_1(\tilde{f}) \sin\tilde{\theta} + b_2(\tilde{f}) \sin 2\tilde{\theta}].\end{aligned} \tag{44}$$

The function $\tilde{Q}(\tilde{f},\tilde{\theta})$ is known from Eqs. (30) and (19), which express linear wave theory. However, relatively slight departures of the observed transfer function from $\tilde{Q}$ can seriously affect the values of the Fourier coefficients. In addition, it is useful to investigate the agreement between the data and linear theory. Therefore, we will replace $\tilde{Q}(\tilde{f},\tilde{\theta})$ by $q(\tilde{f})\tilde{Q}(\tilde{f},\tilde{\theta})$, where $q(\tilde{f})$ is treated as an unknown to be found at the same time as the Fourier coefficients. Its departure from unity will be a measure of the skill of linear theory in explaining the data. Note that this method follows the philosophy of Bowden and White (1966), who used "the observed value of the transfer function" in their analysis of the zero current case.

Inserting Eq. (44) in (38), we find immediately that

$$a_0(\tilde{f}) = 1/\pi. \tag{45}$$

The other five equations will be linear in the five unknowns a_1, a_2, b_1, b_2 and $1/q$ if we make the approximation, good for $q \approx 1$, that

$$(1/q)^2 \approx (2/q) - 1. \tag{46}$$

If higher accuracy is needed, an iterative scheme may be used. Define the notation

$$R(i,j,k) = \int_0^{2\pi} \tilde{Q}^i(\tilde{f},\tilde{\theta}) \sin^j\tilde{\theta} \cos^k\tilde{\theta} d\tilde{\theta}, \quad (47)$$

where the integrals can be evaluated numerically. Then using Eqs. (44)–(47), Eqs. (39)–(43) become

$$a_1R(1,0,2) + a_2[2R(1,0,3) - R(1,0,1)] + b_1R(1,1,1) + b_2[2R(1,1,2)] - q^{-1}c_{\eta V_x}/\tilde{S} = -(1/2\pi)R(1,0,1), \quad (48)$$

$$a_1R(1,1,1) + a_2[2R(1,1,2) - R(1,1,0)] + b_1R(1,2,0) + b_2[2R(1,2,1)] - q^{-1}c_{\eta V_y}/\tilde{S} = -(1/2\pi)R(1,1,0), \quad (49)$$

$$a_1R(2,0,3) + a_2[2R(2,0,4) - R(2,0,2)] + b_1R(2,1,2) + b_2[2R(2,1,3)] - q^{-1}2c_{V_xV_x}/\tilde{S} = -c_{V_xV_x}/\tilde{S} - (1/2\pi)R(2,0,2), \quad (50)$$

$$a_1R(2,1,2) + a_2[2R(2,1,3) - R(2,1,1)] + b_1R(2,2,1) + b_2[2R(2,2,2)] - q^{-1}2c_{V_xV_y}/\tilde{S} = -c_{V_xV_y}/\tilde{S} - (1/2\pi)R(2,1,1), \quad (51)$$

$$a_1R(2,2,1) + a_2[2R(2,2,2) - R(2,2,0)] + b_1R(2,3,0) + b_2[2R(2,3,1)] - q^{-1}2c_{V_yV_y}/\tilde{S} = -c_{V_yV_y}/\tilde{S} - (1/2\pi)R(2,2,0). \quad (52)$$

Eqs. (48)–(52) are solved for a_1, a_2, b_1, b_2 and $1/q$, giving the transformed directional spectrum $\tilde{S}(\tilde{f},\tilde{\theta})$ through Eq. (44). Note that if $\tilde{Q}(\tilde{f},\tilde{\theta})$ were a function of $\tilde{f}$ alone, which would be the case for zero current, the analysis would reduce to that given by Bowden and White (1966).

The series given by Eq. (44) is quite similar to the type of expansion for the spreading function which is possible given the data from a tilt and roll buoy (Longuet-Higgins *et al.*, 1963). Unfortunately, the severely truncated series typically has large negative side lobes which are physically unrealistic. Longuet-Higgins *et al.* (1963) eliminated this problem by introducing a weighting function which effectively smoothed the resulting angular distribution function. This approach has the disadvantage of making the resolution of any distribution narrower than $\cos^4(\theta/2)$ impossible.

The amount of information present in wave height and velocity signals does not permit greater angular resolution than is present in a second-order Fourier expansion. However, if a given functional form for the directional spectrum is assumed, the covariances of the signals can be used to produce very useful information about the parameters of that function. By choosing a physically realistic function form, a smooth spreading function with adequate angular resolution can therefore be obtained.

There have been a few measurements of directional spectra in the ocean which had rather good directional resolution. The classic SWOP study (Chase *et al.*, 1957) analyzed stereo-optical photographs of waves. Tyler *et al.* (1974) used radio backscatter to determine the directional distribution of waves in the 7 s band. Regier (1975) analyzed the data from an array of six wave staffs mounted on the research platform *Flip*. On the basis of these observations, the directional spreading function for a given frequency can be reasonably supposed to be unimodal and symmetrical.

There are a number of functional forms which are smooth and unimodal. Since these functions have similar shapes, it is difficult to decide between them from a study of the data. To facilitate comparisons with previous results, we therefore adopted a commonly used form proportional to $\cos^{2s}[(\theta - \theta_0)/2]$. As s increases, the function becomes more sharply peaked.

The parameter s is determined from the data as follows. The actual functional form to be fit to the data is written as

$$\tilde{H}(\tilde{f},\tilde{\theta}) = \frac{1}{2\sqrt{\pi}} \frac{\Gamma(\tilde{s}+1)}{\Gamma(\tilde{s}+\frac{1}{2})} \cos^{2\tilde{s}}[(\tilde{\theta} - \tilde{\theta}_0)/2], \quad (53)$$

where θ_0 is the direction of the peak and the additional factors have been included to make

$$\int_{-\pi}^{\pi} \tilde{H}(\tilde{f},\tilde{\theta}) d\tilde{\theta} = 1, \quad (54)$$

and the parameters $\tilde{s}$ and $\tilde{\theta}_0$ depend on frequency $\tilde{f}$. To match $\tilde{H}(\tilde{f},\tilde{\theta})$ to the data, we write (53) as a Fourier series of the form

$$\tilde{H}(\tilde{f},\tilde{\theta}) = (1/\pi)[\tfrac{1}{2} + \sum_{n=1}^{\infty} (c_n \cos n\tilde{\theta}_0) \cos n\tilde{\theta} + \sum_{n=1}^{\infty} (c_n \sin n\tilde{\theta}_0) \sin n\tilde{\theta}], \quad (55)$$

where

$$c_n = \frac{\Gamma^2(\tilde{s}+1)}{\Gamma(\tilde{s}+n+1)\Gamma(\tilde{s}-n+1)}. \quad (56)$$

In particular,

$$c_1 = \frac{\tilde{s}}{(\tilde{s}+1)}, \quad (57)$$

$$c_2 = \frac{\tilde{s}(\tilde{s}-1)}{(\tilde{s}+1)(\tilde{s}+2)}. \quad (58)$$

Comparing (55) with (44),

$$\pi a_1 = c_1 \cos\tilde{\theta}_0, \quad (59)$$

$$\pi a_2 = c_2 \cos 2\tilde{\theta}_0, \quad (60)$$

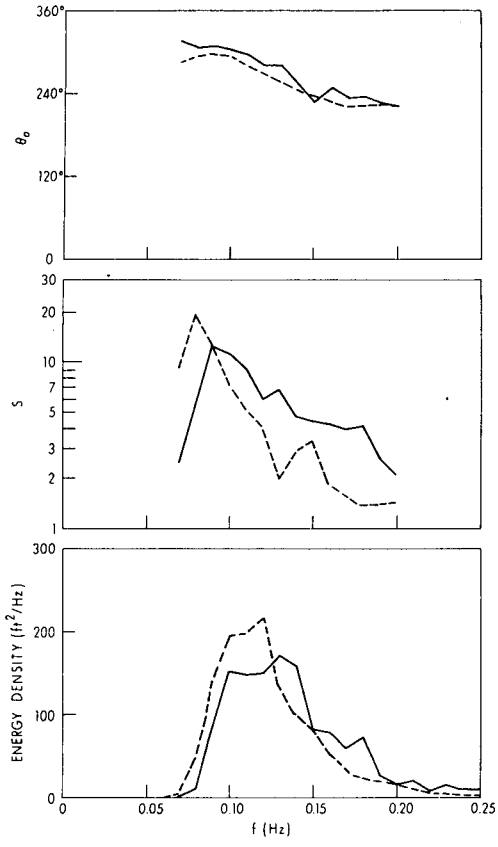

FIG. 9. Directional spectrum at Buccaneer, 1230 CDT 4 September 1973. Solid line: analysis assuming zero current; dashed line: analysis using measured current equal to (−2.98, −5.34) ft s^{-1}.

$$\pi b_1 = c_1 \sin\tilde{\theta}_0, \tag{61}$$

$$\pi b_2 = c_2 \sin 2\tilde{\theta}_0. \tag{62}$$

Thus,

$$\tan\tilde{\theta}_0 = b_1/a_1, \tag{63}$$

$$\tan 2\tilde{\theta}_0 = b_2/a_2, \tag{64}$$

$$c_1^2 = (a_1^2 + b_1^2)\pi^2, \tag{65}$$

$$c_2^2 = (a_2^2 + b_2^2)\pi^2. \tag{66}$$

In practice, only the values calculated from (63) and (65) were used in the analysis, since the values depending on the higher coefficients tended to be somewhat unstable.

Since there were three current meters operating at the station, three independent sets of covariances were available for use in (63) and (65). Actually, combinations of axes from different current meters could be used to further increase the total number of estimates, but this was not done. The results using the records from the three meters were rather similar, but to increase the statistical reliability of the results they were combined by averaging the calculated values of c_1 and c_2. Since the deeper meters would be expected to provide relatively little information on the shorter waves, the averaging used weighting by $\tilde{Q}(\tilde{f},\tilde{\theta})$.

Eq. (57) can be solved for $\tilde{s}$ in terms of c_1 and the directional spreading at each frequency is then given by (53). The directional spectrum in terms of Doppler-shifted frequencies is then given by (44). Eq. (29) can then be used to transform directional spectral densities to their proper value in the frame advecting with the current. If spectral densities at specific frequencies are desired, interpolation can be used. For some purposes, it may be useful to re-parameterize the advecting spectrum in terms of θ_0 and s. This can be done by using a nonlinear curve-fitting routine.

It is appropriate at this stage of the development to discuss some of the details of the procedures actually used in implementing the calculations. For each 30 min segment of data analyzed, 2048-point fast Fourier transforms were taken of concurrent wave and current meter records. Cospectra were formed by multiplication in the frequency domain. The cospectra were smoothed using a Gaussian filter of effective width 0.01 Hz to produce spectra with 20 equivalent degrees of freedom.

An example of the effect of considering the measured current in the calculation of the directional spectrum is shown in Fig. 9. The time shown is 1230 CDT 4 September 1973. The current was equal to (−2.98, −5.34) ft s^{-1}, which was close to the highest measured. For ease of comparison, the spectra are presented in terms of the parameters $S(f)$, $s(f)$ and $\theta_0(f)$. The plots of the three parameters are stacked one above the other with a common frequency scale. Note that because of the functional form of (53), the spreading parameter is displayed on a logarithmic scale.

The results of the analysis assuming no current are shown by solid lines in Fig. 9 and the results using the measured current are shown by dashed lines. The strong current was setting toward 240° true, almost exactly in the same direction as the high-frequency components of the wave spectrum. Therefore, the basic effect of including the current in the analysis is to shift the energy measured in the fixed frame to lower frequencies. The higher peak in the spectrum including the effect of the current is due partly to the shift of energy from higher frequencies and partly to the effect of the transformation factor $(\partial\beta/\partial f)$ in (29). The total energy of variance is preserved by the transformation. The change in shape of the energy spectrum, however, is not negligible. The magnitude of the change, unfortunately, casts some doubt on measurements made from fixed locations when strong unmeasured currents might have existed.

The effect of the current on the other parameters is more difficult to explain in general terms, since

it is the result of transforming many wave components with different frequencies and directions of travel. However, much of the change is clearly related to the red shift of almost all components in the spectrum. The highest values of s still occur near the low-frequency peak of the energy spectrum, a feature noted by many previous investigators, in particular, Mitsuyasu *et al.* (1975). That is, the energy at the peak of the spectrum has the narrowest directional spread.

This single example of a measured directional spectrum shows that the directional characteristics of the wave spectrum in a tropical storm are very complicated. Waves with different frequencies also have different spreading and different main directions of travel. Thus, efforts toward producing a simple parameterization of directional spectra in storms seem futile.

c. *Fit of the data to linear directional theory*

As mentioned in the development above, the accuracy of linear theory in explaining the measured velocity data can be checked by examination of the transfer function correction $q(\tilde{f})$. Recall that if $q(\tilde{f}) = 1$, the data is best fit by linear theory. Thus, the factor $q(\tilde{f})$ can be thought of as the ratio between the measured velocity and that predicted by linear theory. These ratios are shown for the three current meters in Fig. 10. In general, the performance of linear theory is quite good, with agreement almost always better than 10% for the frequencies at which most of the wave energy is concentrated. The agreement shows that linear theory certainly can be applied in calculating directional spectra and that linear directional theory is much more successful in explaining the data than higher order unidirectional theories which had significant bias.

However, the detailed structure of the discrepancies between linear theory and the data may still be of some interest. The ratios were constant neither in frequency nor time through the storm, although the same trends continued to be observed. The general trend was toward overprediction at higher frequencies, followed at the lower meters by a decrease in signal-to-noise ratio and underprediction at frequencies high enough for the transfer function to be very small. The visual correlation of the ratios across depth was rather high. All of these facts argue that the discrepancies cannot be explained completely by current meter calibration errors, but are instead probably due to nonlinear phase locking effects between harmonics. Further study of this type of data may shed some light on nonlinear effects in random directionally spread seas.

The trends with frequency shown in Fig. 10 show some similarity with the results presented by Thornton and Krapohl (1974). Their Fig. 5 shows

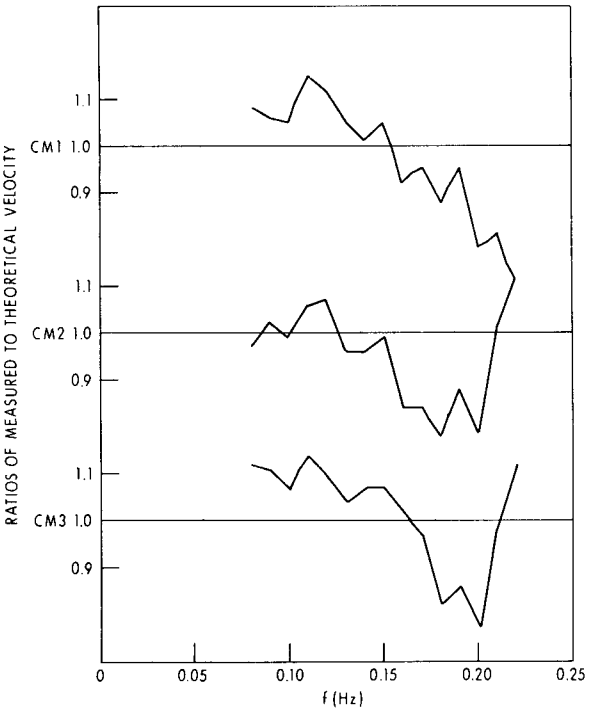

FIG. 10. Ratio of measured to theoretical velocity at Buccaneer, 1200 CDT 4 September 1973.

that the measured velocity slightly exceeded the theoretical velocity for the energetic low-frequency range of the spectrum. Then in an intermediate range, the measurements were roughly equal to the theory. Finally, above about 0.23 Hz the measurements became much greater than the theoretical predictions. Cavalieri *et al.* (1977) showed measured velocities slightly less than predicted by linear theory over the range 0.15–0.25 Hz.

Despite the probable existence of nonlinear effects in the data, it is clear that linear theory provides sufficient accuracy for many purposes and is more accurate than unidirectional theories which include nonlinear effects. Since the linear transfer function between wave surface and particle velocity is correct to a good degree of approximation, (7) and (8) can be used to predict the velocity spectra when the directional wave spectra are known. This procedure will be directly useful in some practical problems where the force on a structure may be approximated by a linear transfer function from the kinematics of the flow. We will see in a later section that the use of linear theory also permits calculation of the probability distribution function of velocities and that these distributions closely approximate the observed distributions.

6. Hindcasting the directional spectra

In order to use directional spectra in design, we must have a method of hindcasting directional

spectra from historical wind field data. A numerical hindcasting scheme designed specifically for hurricanes has been developed by Cardone *et al.* (1976) and calibrated with measured frequency spectra for Gulf of Mexico hurricanes. The Delia data represent the first opportunity to check the model against directional spectra measured in a tropical storm.

There are two major aspects to the wave hindcasting model: the wind field description and the wave prediction technique. The importance of the wind field description cannot be overemphasized. For hurricanes, it is possible to use a model storm approach, since the similarity of hurricane pressure fields allows their description with relatively few parameters. This is fortunate, since the sparseness of measurements in most hurricanes precludes the use of standard synoptic meteorological analysis techniques.

The wind field model used is an application of the theoretical model of the horizontal air flow in the boundary layer of a moving vortex as originally derived by Chow (1971). The pressure field is prescribed as the sum of an axially symmetric part, parameterized by the central pressure and a scale radius, and a large-scale pressure field with constant gradient. The equations of motion averaged over the boundary layer depth are then numerically integrated. Several solutions are typically made to describe the storm at various stages of its development and then interpolation along the storm track is used to produce wind fields at each time needed by the wave program.

The wave prediction model is a rather straightforward application and calibration of the model of Pierson *et al.* (1966) which simulates the process of wave growth, dissipation and propagation on a hexagonal grid system consisting of 1694 points spaced 35 km apart. At each grid point, the directional spectrum is resolved into 13 frequency and 24 direction bands. The growth algorithm, applied to spectral components traveling within 90° of the wind direction, parameterizes the linear and exponential growth of energy associated with the mechanisms proposed by Phillips (1957) and Miles (1959), respectively. Spectral components traveling against the wind are attenuated at a rate proportional to the fourth power of the frequency and the energy of the local wind sea. Propagation of spectral components in deep water is accomplished by a simple Lagrangian scheme. In shallow water, the effects of refraction, shoaling and bottom friction are included.

A rather different approach to numerical wave hindcasting has been proposed recently by Hasselmann *et al.* (1976) who contend that the evaluation of the wave spectrum in a generating situation is dominated by energy transfers across the spectrum associated with nonlinear resonant wave-wave interactions. Since the incorporation of such a mechanism rigorously in a numerical hindcast model is impossible with present computer speeds, Hasselmann *et al.* (1976) proposed a new structure for hindcast models based on the hypothesis that the nonlinear interactions act to stabilize the spectral shape. The shape invariance with the stage of wave development is exploited by the representation of the frequency spectrum in terms of a small (1–5) number of parameters and the derivation of a set of simpler prognostic equations for the parameters. The directional spread of energy is fixed for all frequencies and is assumed concentrated about the local wind direction.

It was recognized by Hasselmann *et al.* (1976) that the simple parametric models proposed may not work in meteorological systems involving rapidly changing wind fields (e.g., hurricanes) and they suggest that hybrid models which model wave growth and dissipation in parametric space and which track swell resolved in spectral bands would be necessary. While such models are under development (e.g., Gunther and Rosenthal, 1977; Weare and Worthington, 1977) there remain formidable problems such as the simulation of sea-swell energy transfers and the simulation of the spectral energy balance in the late stages of wave development.

The hindcast model applied here to Delia includes nonlinear effects in a highly implicit way. The Pierson-Moskowitz (1964) fully developed form of the frequency spectrum, coupled to a frequency-dependent functional form for the angular spread of energy, is used to limit wave growth. As shown by Pierson (1977), in simple, offshore, fetch-limited wave generation, the growth algorithm simulates features such as the migration of the spectral peak toward lower frequency and a decrease in spectral peak sharpness with increasing fetch which have been attributed to nonlinear effects. Also, in regions of rapidly turning winds, spectral energy is redistributed angularly in the growth algorithm to simulate the known tendency for the peak in the directional spectrum to track the local wind direction, albeit with lag, which is an effect probably caused by nonlinear interactions. Finally, the linear and exponential growth rates employed in the model are calibrated against measurements of net wave growth and therefore include contributions to growth of the forward face of the spectrum associated with weak wave-wave interactions.

Study of hurricane Camille led to some modification of the parameterizations of the growth-dissipation calculations which were most important for very high winds. These modifications led to a model which accurately hindcast the significant wave height and power spectra during several measured hurricanes (Cardone *et al.*, 1976).

The wind field used to hindcast the directional spectra in Delia was the same as that used by

Forristall *et al.* (1977) to hindcast the wind-driven currents in Delia. The storm track, central pressure analysis, and comparisons of measured and hindcast wind speed and direction may be found in that reference.

The first level in the verification of the wave hindcast results is a comparison between the measured and hindcast total variance. For ease of interpretation, we have actually displayed the approximation to the significant wave height given by four times the square root of the variance in Fig. 5. The measurements are given by the dashed line and the hindcast results by the dotted line. The hindcast results are generally higher than the data by about 2 ft and the peak of the hindcast leads the peak of the data by 1 h. Part of the reason for the discrepancy may be due to the placement of the model grid points with respect to the Buccaneer station and the storm track as shown in Fig. 11. The comparisons have all been made using results from grid point 1350, which the storm track approached sooner and nearer. Note that the very large radius to maximum winds in Delia meant that the wind speed at Buccaneer actually began declining about 1200 CDT.

The measured directional spectra are compared to the hindcasts in Figs. 12–14 for 0800, 1200 and 1500 CDT, respectively. For ease in comparison, both the measured and hindcast spectra have been fit to the spreading function given by (53) by using a nonlinear curve-fitting program. The measured spectra are given by the solid lines and the hindcasts by the dashed lines. In addition, the dotted line in Fig. 13 shows the spectrum measured at 1300, so that the peak measured spectrum can be compared with the peak hindcast spectrum.

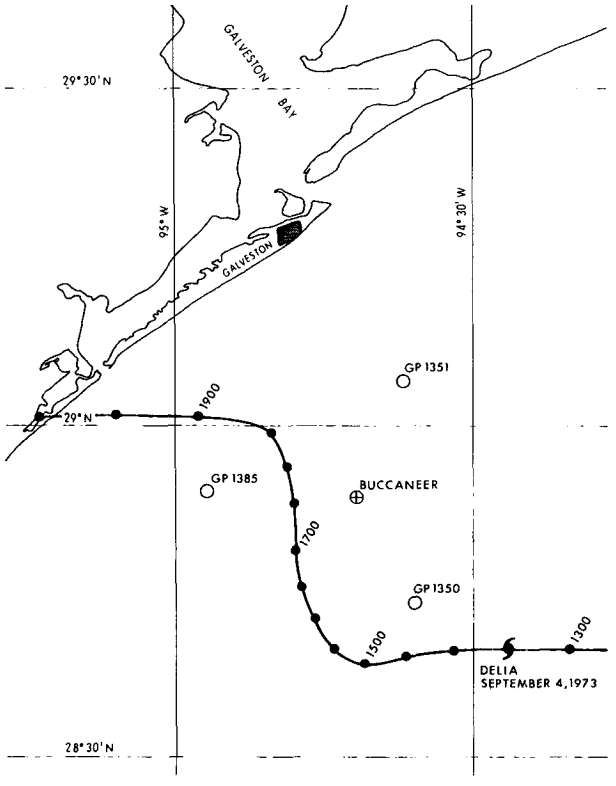

FIG. 11. Detailed storm track for Delia near Buccaneer and the surrounding hindcast grid points.

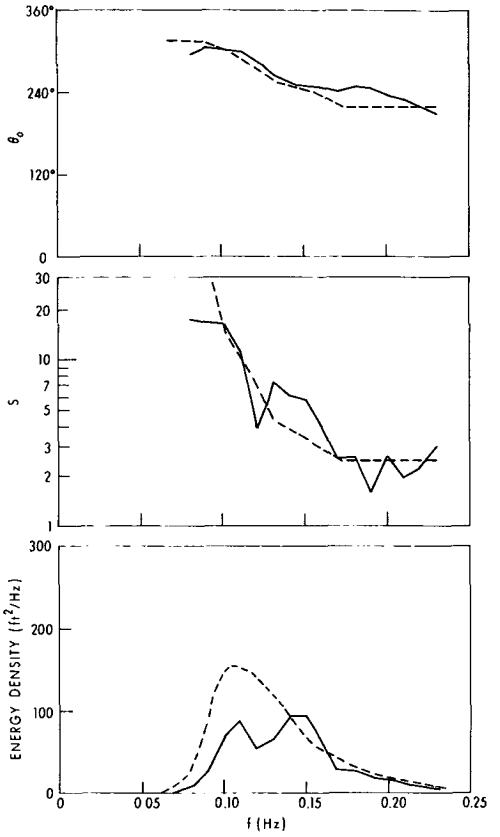

FIG. 12. Directional spectrum at Buccaneer, 0800 CDT 4 September 1973. Solid line: measurements; dashed line: hindcast.

The positive bias in total energy in the hindcasts is associated with too much low-frequency energy. It is possible that this discrepancy is related to some unmodeled wave-current interaction or to attenuation associated with wave-bottom interactions that are stronger than modeled. The match of the high-frequency energy and the fit of the peak storm spectra are, however, quite good. The hindcasts of the directional parameters of the spectra are excellent, particularly considering the dearth of previous calibration of the directional features of the hindcast model.

The directional spectra give a fascinating view of the development of the sea state as a tropical storm approached. The low-frequency energy around 0.10 Hz propagates as swell from near the center of the storm. Since the storm track had an average bearing

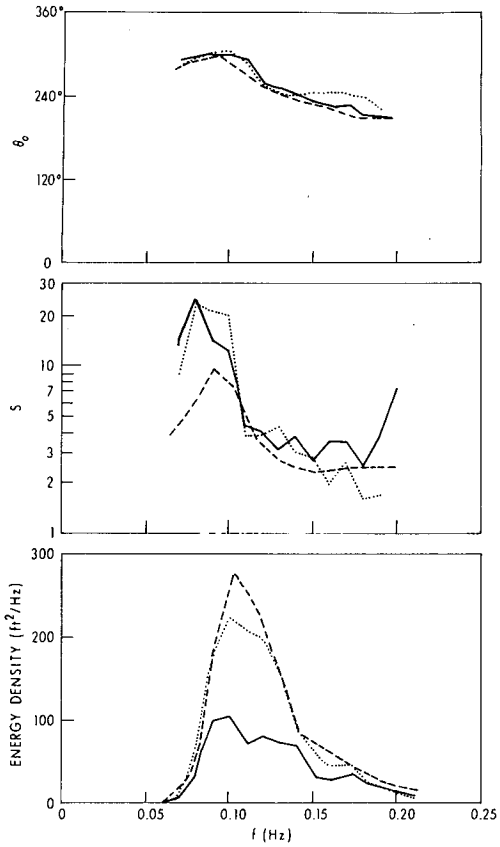

FIG. 13. As in Fig. 12 except at 1200–1300 CDT. Solid line: measurements at 1200 CDT; dashed line: hindcast at 1200 CDT; dotted line: measurements at 1300 CDT.

of about 300°, both the measured and hindcast directions of propagation for the low-frequency components stay near 300° throughout the storm period shown. The hindcasts also match the observed narrow directional spread of the low-frequency components.

In contrast, the higher frequency waves generated by the local wind are much more spread and tend to follow the changes in the local wind direction. The energy at 0.20 Hz was propagating toward 240° at 0800, swinging to 210° at 1200 and then back to 265° at 1500, as the storm center rounded the platform. The hindcast directions at this frequency are in good agreement, but the model seems to react to shifts in the wind direction a bit more quickly than does nature.

In between the low and high frequencies discussed above, the directional properties show a smooth transition which is closely matched by the hindcast. In summary, the directional spectral model produced a much better fit to the data than could be hoped for with any simple spectral parameterization or simple parameter hindcast model based thereon. This agreement, coupled with the previous agreement between hindcast and measured energy spectra during more severe seas (Cardone *et al.*, 1976), strongly suggests that the directional spectra of severe seas can be satisfactorily hindcast for use in design applications.

7. Velocity probability distributions

We have seen that the spectra of the measured velocities can be explained using linear wave theory and that the directional wave spectrum can be estimated from the measurements. Knowledge of the velocity spectra is useful for some design problems, particularly those involving fatigue. However, design work also requires information about the peak waves to be expected and the spectrum provides no direct measure of the extremes. Fortunately, by analogy with methods of estimating wave height distributions, it is possible to develop a formula for the probability distribution of the velocity. This distribution can then be compared with the measured extreme value distribution to show that directional spreading of linear waves can account for the extreme velocities measured as well as accounting for the velocity spectra.

If the phase angles in Eq. (5) have a uniform random distribution, then the surface elevation η will

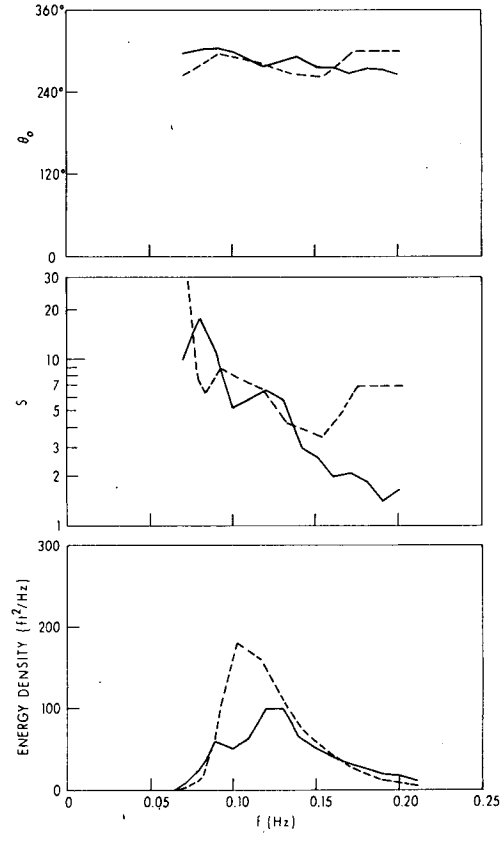

FIG. 14. As in Fig. 12 except 1500 CDT.

have a Gaussian distribution with mean zero and standard deviation equal to the total variance of the spectrum. The distribution in the fixed measurement frame of reference will be the same as the distribution in the frame moving with the current. The Gaussian distribution of surface elevations is commonly observed, although sometimes nonlinear effects are observable (Longuet-Higgins, 1963). By the form of the summations for the velocity components in (7) and (8), it is obvious that they too will have Gaussian distributions, with standard deviations for the x and y components given, respectively, by

$$\alpha_x^2 = \sum_m \sum_n S_{mn}\Delta f\Delta\theta 4\pi^2 f_m^2 \frac{\cosh^2 k_m z}{\sinh^2 k_m d}\cos^2\theta_n, \quad (67)$$

$$\alpha_y^2 = \sum_m \sum_n S_{mn}\Delta f\Delta\theta 4\pi^2 f_m^2 \frac{\cosh^2 k_m z}{\sinh^2 k_m d}\sin^2\theta_n. \quad (68)$$

The prediction of Gaussian velocity component distributions can be checked by using the measured directional spectrum to evaluate (67) and (68) and comparing the theoretical distributions with those measured. Fig. 15 shows the distributions for the upper current meter during the hour beginning at 0600 CDT plotted on a normal probability scale. The theoretical normal distributions are thus straight lines. The fit is generally very good, except that the positive tail of the distributions for V_y is higher than theoretically predicted. At this time, the wave energy was propagating in a generally westward direction such that most of the high positive velocities occurred under the troughs of waves. Thus, this discrepancy is consistent with the results in Fig. 6.

The fit of a Gaussian distribution to the velocity components is encouraging and certainly better than the fit of regular wave theories to individual waves as shown in Fig. 6. However, to compare results more directly with the regular wave fits, it would be useful to have the distribution of the peak velocity magnitudes (speeds). The analysis will also show that this distribution is particularly practical, since it is independent of most of the details of the directional spectra.

Longuet-Higgins (1952) has studied the closely related problem of the distribution of the heights of waves. There exists some function $B(t)$ such that the representation of Eq. (4) can be written

$$\eta(0,0,t) = \cos(2\pi f_0 t)B(t). \quad (69)$$

This is a carrier wave of frequency f_0 modulated by an envelope function $B(t)$. When the spectrum of $\eta(t)$ is concentrated in a narrow frequency band, Longuet-Higgins showed that the distribution of the amplitudes is equal to the distribution of the function $B(t)$. Further, the probability density function of $B(t)$ was shown to be Rayleigh with parameter α^2 equal to the zeroth moment of the spectrum of η. The Rayleigh distribution for wave heights has been shown to be reasonably accurate when checked against actual storm waves, although there is some overprediction of the highest waves, probably due to the nonlinearity of the real sea (Forristall, 1978).

By similarity of form, it is obvious that the distribution of velocity component peaks should also be Rayleigh, with parameters given by (67) and (68).

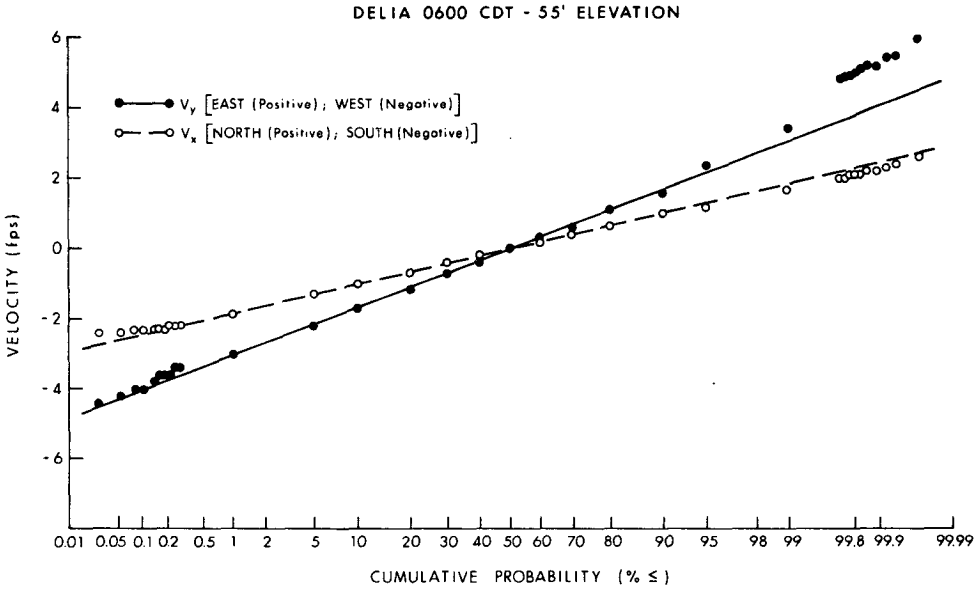

FIG. 15. Cumulative probability of velocity components. Lines are from linear theory, points are measurements.

The speed S of the water is the magnitude of the velocity. Thus

$$S = (V_x^2 + V_y^2)^{1/2}. \quad (70)$$

If, following Longuet-Higgins, we write

$$V_x = \cos(2\pi f_0 t)B_x(t), \quad (71)$$

$$V_y = \cos(2\pi f_0 t)B_y(t), \quad (72)$$

then

$$S = \cos(2\pi f_0 t)[B_x^2(t) + B_y^2(t)]^{1/2}, \quad (73)$$

and the distribution of the speed peaks will be the same as the distribution of the envelope function in brackets.

Some well-known methods for combining probability distributions could be used to calculate the distribution of S, provided $B_x(t)$ and $B_y(t)$ are independent. This is not necessarily true. For example, if the wave spectrum is unidirectional at angle θ, then

$$V_y = \tan\theta V_x. \quad (74)$$

However, there exists a coordinate system (a,b) in which V_a and V_b are statistically independent. The angle of rotation between the (a, b) coordinates and the (x,y) coordinates is given by:

$$\tan 2\theta = 2C_{V_xV_y}/(C_{V_xV_x} - C_{V_yV_y}). \quad (75)$$

In the (a,b) coordinate system, theorems (e.g., Parzen, 1960) for finding the distributions of squares and sums of independent random variables may be used. First, if

$$Z_a = B_a^2, \quad (76)$$

then Z_a has a probability density function given by:

$$F_{Z_a}(z_a) = (2\alpha_a^2)^{-1} \exp(-z_a/2\alpha_a^2). \quad (77)$$

Then, if $Z = Z_a + Z_b$, the probability density of Z is given by the convolution of the density functions for Z_a and Z_b or

$$f_Z(z) = \int_0^z f_{Z_a}(z - x)f_{Z_b}(x)dx = [2(\alpha_b^2 - \alpha_a^2)]^{-1} \times [\exp(-z/2\alpha_b^2) - \exp(-z/2\alpha_a^2)]. \quad (78)$$

Now, since the distribution of S is the same as that of $(Z)^{1/2}$, the density function of S is

$$f_S(S) = \frac{S}{\alpha_a^2 - \alpha_b^2}\{e^{-S^2/2\alpha_a^2} - e^{-S^2/2\alpha_b^2}\}, \quad (79)$$

and its distribution function is

$$F_S(S) = 1 - \{(\alpha_a^2 - \alpha_b^2)^{-1}[\alpha_a^2 \exp(-S^2/2\alpha_a^2)] - \alpha_b^2 \exp(-S^2/2\alpha_b^2)]\}. \quad (80)$$

We now define

$$\alpha^2 = \alpha_a^2 + \alpha_b^2 = \alpha_x^2 + \alpha_y^2, \quad (81)$$

and define the spreading factor c by

$$c = \alpha_a^2/\alpha^2, \quad (82)$$

where the rotation was taken such that $\alpha_a \geq \alpha_b$. If the speed is normalized so that

$$\xi = S/\alpha, \quad (83)$$

then Eq. (80) can be reduced to a parametric distribution dependent only on the spreading factor, i.e.,

$$F(\xi) = 1 - \left(\frac{c}{2c - 1}\right)\exp(-\xi^2/2c) + \left(\frac{1 - c}{2c - 1}\right)\exp[-\xi^2/2(1 - c)]. \quad (84)$$

This distribution has been plotted for three values of c in Figs. 16–18. If the waves are unidirectional, $c = 1$; $c = 0.5$ would be produced by omnidirectional waves. By a rather complicated derivation, it can be shown that $c = 0.75$ would be produced by spreading of the form given by (53) with $s = 5.33$ and the same θ_0 for all frequency bands. Since we are primarily interested in the tail of the distribution, the figures actually show the probability of exceedance of a given normalized speed which is given by $1 - F(S/\alpha)$. By way of example, for $c = 1$, which is of course a Rayleigh distribution, the probability that a speed peak will exceed 3.03α is 1/100.

To find the spreading factor given a complicated measured or hindcast directional spectrum, it is necessary to rotate the velocity variances into the (a, b) coordinate system. This can be done using a Mohr's circle construction (a tensor transformation) to get

$$\alpha_a^2 = C_{V_aV_a} = \tfrac{1}{2}(C_{V_xV_x} + C_{V_yV_y}) + r, \quad (85)$$

$$\alpha_b^2 = C_{V_bV_b} = \tfrac{1}{2}(C_{V_xV_x} + C_{V_yV_y}) - r, \quad (86)$$

where

$$r^2 = \tfrac{1}{4}(C_{V_xV_x} - C_{V_yV_y})^2 + C_{V_xV_y}^2. \quad (87)$$

The values of c during Delia were mostly in the range $c = 0.70$ to $c = 0.75$, with the values at the bottom meter somewhat higher. Thus, there is justification for lumping together the measurements from several hours by normalizing by the variance α.

To compare the predicted and measured distributions, the x and y particle velocities were combined using (70). Then, the peaks of the speed trace were selected from 1 h segments of the records and ranked in descending order. Note that there are two peaks of the speed trace per wave cycle, one associated with the wave crest and one with the wave trough. The association of peaks with either crests or troughs is not preserved in this type of analysis.

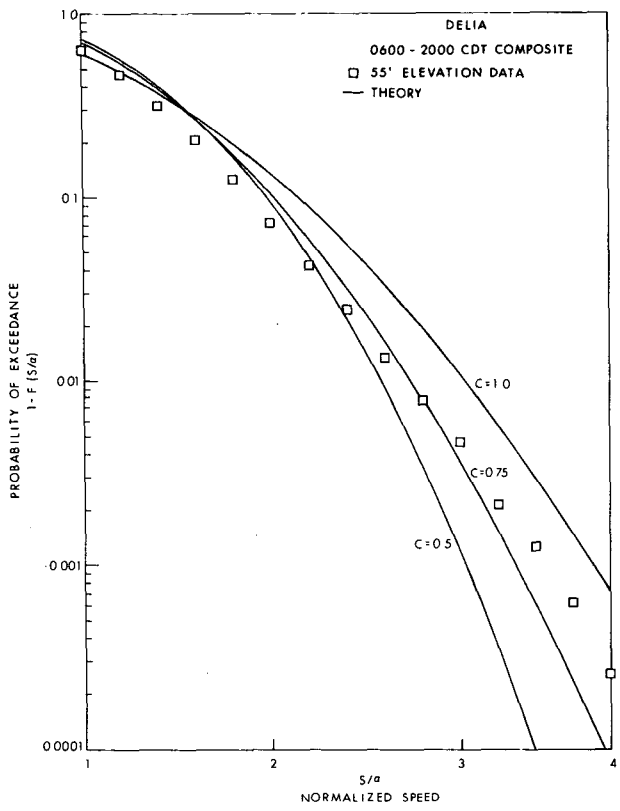

FIG. 16. Composite speed peak distribution for top meter.

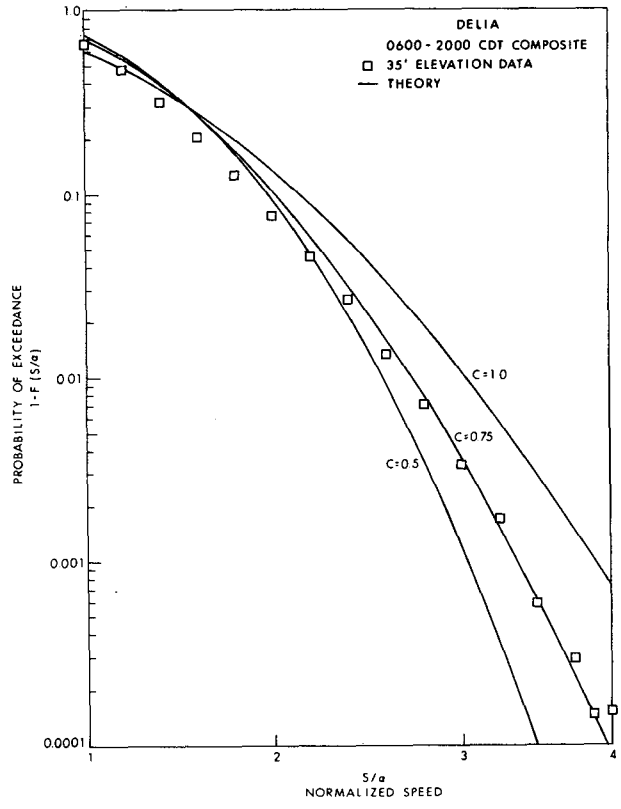

FIG. 17. Composite speed peak distribution for middle meter.

Additionally, it is necessary to know the number of speed maxima in a given hour to compute probabilities. Of course, this is known directly from the observed velocities, but it would not be known in the historical hindcast case and, in practice, the speed data contain many small maxima probably related to turbulence or noise rather than surface waves. Thus, it is desirable to have an independent estimate of the number of speed maxima in an hour. It has been found that the number of surface waves in a time interval is well approximated by the ratio of the first to the zeroth moment of the wave spectra times the length of the time interval. A similar estimate can be made from the moments of the theoretical velocity spectra at various depths, accounting for the fact that there will be twice as many speed maxima as waves. Our comparisons proceeded on this basis.

The speed peak distributions for the three current meters over the period 0600–2000 CDT are shown in Figs. 16–18. The distributions at the top two meters agree remarkably well with the theory at a spreading factor of 0.75, while the distribution at the bottom meter is somewhat higher. This is consistent with the greater attenuation of higher frequency energy components with depth.

It is interesting to note from Figs. 16 and 18 that the distribution corresponding to unidirectional

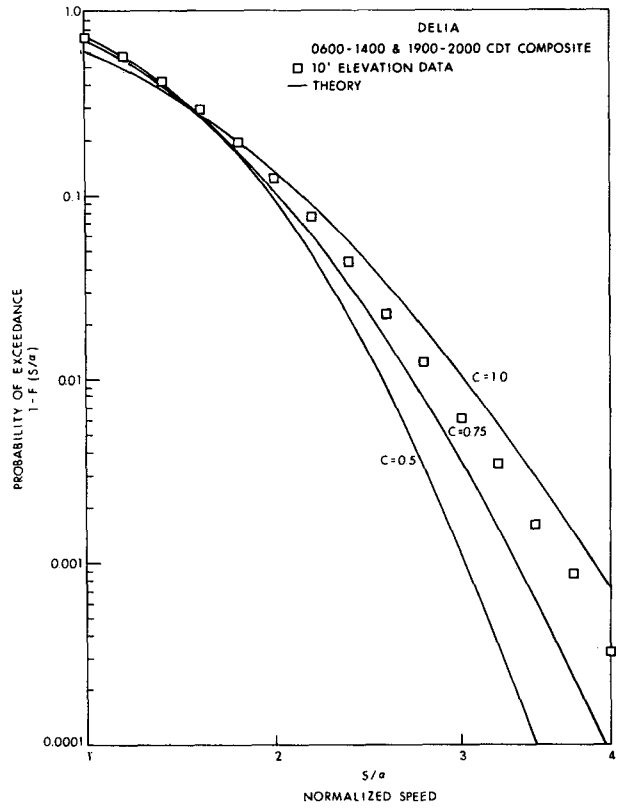

FIG. 18. Composite speed peak distribution for bottom meter.

theory ($c = 1$) would over-predict the water speed at the tail of the distributions by about 10%. However, when unidirectional wave theory was applied on a wave by wave basis to the highest waves, we saw that the overprediction was as much as 40% under wave crests. The reason for this seeming discrepancy can be traced to the nature of a directionally spread sea. Just as the wavelets that add to produce the highest waves do not necessarily add colinearly in velocity, the wavelets which add to produce the highest speeds do not necessarily produce the largest wave height. In other words, in a directionally spread sea, the highest particle velocities do not necessarily occur under the highest waves.

8. Conclusions

The waves measured in Tropical Storm Delia were directionally spread. Thus, the use of unidirectional wave theory to calculate water particle velocities results in both random and systematic errors. However, the use of linear wave theory along with the concept of the directional spectrum succeeded in predicting both the spectra and extreme value statistics of the measured velocities. Although effects of nonlinearities were undoubtedly present, the assumption of linearity has been shown to be less damaging than the assumption of unidirectionality. A numerical wave model was also successful in hindcasting the observed directional spectra.

For some design problems, it will be possible to use hindcast directional spectra from historical storms directly to calculate either the spectra or extreme value distributions of the velocities. However, for large space frame structures, it will probably be more practical to simulate the velocities and accelerations from the hindcast directional spectrum using linear theory and a Monte Carlo randomization of the phase angles.

Acknowledgments. The data on which this work is based would not have existed without the dedication and hard work of R. C. Hamilton and T. E. Long. C. A. Gutierrez did much of the computer programming for the data analysis. R. P. Nordgren, A. M. Reece and M. E. Thro made helpful comments on earlier versions of the manuscript. The data collection program was executed by Shell Development Company with financial support from Amoco Production Research, Chevron Oil Field Research Company, Exxon Production Research Company, Mobil Research and Development Company, and Seadock, Inc.

REFERENCES

Bowden, K. F., and R. A. White, 1966: Measurements of the orbital velocities of sea waves and their use in determining the directional spectrum. *Geophys. J. Roy. Astron. Soc.*, **12**, 33–54.

Cardone, V. J., W. J. Pierson, and E. G. Ward, 1976: Hindcasting the directional spectra of hurricane-generated waves. *J. Petrol. Tech.*, **25**, 385–394.

Cartwright, D. E., 1963: *The Use of Directional Spectra in Studying the Output of a Wave Recorder on a Moving Ship, Ocean Wave Spectra*. Prentice-Hall, 203–218 pp.

Cavaleri, L., J. A. Ewing and N. D. Smith, 1977: Measurement of the pressure and velocity field below surface waves. Paper presented at the NATO Symposium on Turbulent Fluxes through the Sea Surface, Ile de Bendor, France.

Chappelear, J. E., 1961: Direct numerical calculation of wave properties. *J. Geophys. Res.*, **66**, 501–508.

Chase, J., L. J. Cote, W. Marks, E. Mehr, W. J. Pierson, F. G. Ronne, G. Stephenson, R. C. Vetter and R. G. Walden, 1957: The directional spectrum of a wind-generated sea as determined from data obtained by the stereo wave observation project. New York University, College of Engineering, Dept. of Meteorology and Oceanography and Engineering Statistics Group, Tech. Rep. ONR Contract Nonr 285(3), 267 pp.

Chow, S., 1971: A study of the windfield in the planetary boundary layer of a moving tropical cyclone. M.S. thesis, Dept. of Meteorology and Oceanography, New York University, 58 pp.

Dean, R. G., 1965: Stream function representation of nonlinear ocean waves. *J. Geophys. Res.*, **70**, 4561–4572.

Forristall, G. Z., 1978: On the statistical distribution of wave heights in a storm. *J. Geophys. Res.*, **83**, 2353–2358.

——, V. J. Cardone and R. C. Hamilton, 1977: Continental shelf currents in Tropical Storm Delia: Observations and Theory, *J. Phys. Oceanog.*, **7**, 532–546.

Gunther, H., and W. Rosenthal, 1978: Parametrical numerical wave prediction tested in wind situations varying in time and space. *Proc. NATO Symp. on Turbulent Fluxes through the Sea Surface, Wave Dynamics and Prediction*, Ile de Bendor, France, Plenum Publ. Co. (in press).

Hasselmann, K., D. B. Ross, P. Müller and W. Swell, 1976: A parametric wave prediction model. *J. Phys. Oceanogr.*, **6**, 200–228.

Jahns, H. O., and J. D. Wheeler, 1973: Long-term wave probabilities based on hindcasting of severe storms. *J. Petrol. Tech.*, **25**, 473–486.

Lambrakos, K. F., and H. R. Brannon, 1974: Wave force calculations for Stokes and non-Stokes waves. *Proc. Sixth Annual Offshore Tech. Conf.*, OTC Paper 2039, 47–60.

Longuet-Higgins, M. S., 1952: On the statistical distribution of the heights of sea waves. *J. Marine Res.*, **11**, 266.

———, 1963: The effect of nonlinearities on statistical distributions in the theory of sea waves. *J. Fluid Mech.*, **7**, 459–480.

——, and R. W. Stewart, 1960: Changes in the form of short gravity waves on long waves and tidal currents. *J. Fluid Mech.*, **8**, 565–581.

——, D. E. Cartwright and N. D. Smith, 1963: Observations of the directional spectrum of sea waves using the motions of a floating buoy. *Ocean Wave Spectra*, Prentice-Hall, 111–136.

Miles, J. W., 1959: On the generation of surface waves by shear flows. Part 2. *J. Fluid Mech.*, **6**, 583–598.

Mitsuyasu, J., F. Tasai, T. Suhara, S. Mizuno, M. Ohkusu, T. Honda and K. Rikiishi, 1975: Observations of the directional spectrum of ocean waves using a cloverleaf buoy. *J. Phys. Oceanogr.*, **5**, 750–760.

Nagata, Y., 1964: The statistical properties of orbital wave motions and their application for the measurement of directional wave spectra. *J. Oceanogr. Soc. Japan*, **19**, 169–181.

Parzen, Emanuel, 1960: *Modern Probability Theory and Its Application*. Wiley, 464 pp.

Phillips, O. M., 1957: On the generation of waves by turbulent wind. *J. Fluid Mech.*, **2**, 417–445.

——, 1977: *The Dynamics of the Upper Ocean*. Cambridge University Press, 336 pp.

Pierson, W. J., 1977: Comments on "A parametric wave prediction model." *J. Phys. Oceanogr.*, **7**, 127–134.

——, and L. Moskowitz, 1964: A proposed spectral form for fully developed wind seas based on the similarity theory of S. A. Kitaigorodskii. *J. Geophys. Res.*, **69**, 5181–5190.

——, L. J. Tick and L. Baer, 1966: Computer based procedures for preparing global wave forecasts and wind field analyses capable of using wave data obtained by a spacecraft. *Proc. Sixth Naval Hydrodynamics Symposium*, Washington, DC, Office of Naval Research, 499–532.

Regier, L., 1975: Observations of the power and directional spectrum of oceanic surface waves. Ph.D. thesis, University of California, San Diego, 176 pp.

Simpson, J. H., 1969: Observation of the directional characteristics of waves. *Geophys. J. Roy. Astron. Soc.*, **17**, 93–120.

Stewart, R. H., and J. W. Joy, 1974: HF radio measurements of surface currents. *Deep-Sea Res.*, **21**, 1039–1049.

Thornton, E. B., and R. F. Krapohl, 1974: Water particle velocities measured under ocean waves. *J. Geophys. Res.*, **79**, 847–852.

Tyler, G. L., C. C. Teague, R. H. Stewart, A. M. Peterson, W. H. Munk and J. W. Joy, 1974: Wave directional spectra from synthetic aperture observations of radio scatter. *Deep-Sea Res.*, **21**, 989–1016.

Weare, T. J., and B. A. Worthington, 1978: A numerical model hindcast of severe wave conditions for the North Sea. *Proc. NATO Symp. Turbulent Fluxes through the Sea Surface, Wave Dynamics and Prediction*, Ile de Bendor, France, Plenum Publ. (in press).

Weber, B. L., and D. E. Barrick, 1977: On the nonlinear theory for gravity waves on the ocean's surface, Part I: Derivations. *J. Phys. Oceanogr.*, **7**, 3–10.

Wheeler, J. D., 1970: Method for calculating forces produced by irregular waves. *J. Petrol. Tech.*, **22**, 473–486.